



1 **Climate-driven biogenic emissions alleviate the impact of man-made emission**

2 **reduction on O₃ control in Pearl River Delta region, southern China**

3 Nan WANG^{1,2*}, Song LIU¹, Jiawei XU³, Yanyu WANG², Chun LI¹, Hua LU^{4*}, Fumo

4 YANG¹

5 ¹College of carbon Neutrality Future Technology, Sichuan University, Chengdu 610065, P. R.

6 China

7 ²State Environmental Protection Key Laboratory of Formation and Prevention of Urban Air

8 Pollution Complex, Shanghai Academy of Environment Sciences, Shanghai 200233, P. R.

9 China

10 ³Centre for Geography and Environmental Science, University of Exeter, Penryn, United

11 Kingdom

12 ⁴Chongqing Institute of Meteorological Sciences, Chongqing 401147, P. R. China

13

14 ***Correspondence:** WANG Nan (nan.wang@scu.edu.cn) and LU Hua

15 (vibgyor0113@163.com)

16



17 **Key Points**

18 1. Summer O₃ concentrations in the Pearl River Delta region is increasing over the
19 past decade.

20 2. Climate-driven BVOC emissions take up ~ 80% of the total increasing BVOC
21 emissions from 2001 to 2020.

22 3. The rising BVOC emissions serve as a key factor in the unexpected rise of O₃
23 levels.

24

25

26

27

28



29 **Abstract**

30 O₃ concentrations in the Pearl River Delta (PRD) during summer are typically low and
31 often overlooked. However, integrated observational data reveal a consistent increase
32 in summer O₃ levels over recent decades (+0.96 ppb/year), contradicting China's efforts
33 to reduce anthropogenic emissions. Our dynamically calculated natural emissions show
34 that biogenic volatile organic compound (BVOC) emissions in the region significantly
35 increased between 2001 and 2020, primarily due to climate change and alterations in
36 vegetation cover, with climate-driven BVOC emissions accounting for approximately
37 80% of the increase. Furthermore, parallel simulations using the WRF-CMAQ model
38 indicate that climate-driven BVOC emissions, by enhancing atmospheric oxidative
39 capacity and accelerating O₃ formation, have weakened or even offset the benefits of
40 anthropogenic emission reductions, contributing 6.2 ppb to O₃ formation and leading
41 to an unexpected rise in O₃ levels. This study enhances our understanding of the
42 mechanisms behind natural emissions in urban O₃ formation under climate change and
43 provides insights for future O₃ pollution control strategies.

44

45

46

47

48 **Key words:** BVOC emission, O₃ pollution, climate impact

49

50



51 **Plain Language Summary**

52 This study examines the rising levels of ozone (O₃) pollution in the Pearl River Delta
53 (PRD) region during summer, a time when O₃ concentrations are typically low. Despite
54 efforts by China to reduce pollution from human activities, our research shows that O₃
55 levels have consistently increased over the past few decades. We found that emissions
56 of biogenic volatile organic compounds (BVOC) from plants have significantly risen
57 from 2001 to 2020, mainly due to climate change and changes in vegetation. Notably,
58 about 80% of this increase in BVOC emissions is driven by climate factors. Our
59 simulations suggest that these climate-driven BVOC emissions are counteracting the
60 benefits of efforts to reduce human-made emissions, contributing significantly to O₃
61 formation. This research helps us understand how natural emissions influence urban O₃
62 levels, particularly under changing climate conditions, and provides valuable insights
63 for future pollution control strategies.



64 **Introduction**

65 Tropospheric ozone (O_3) is formed through photochemical reactions involving its
66 precursors, volatile organic compounds (VOCs), carbon monoxide (CO) and nitrogen
67 oxides (NO_x), under ultraviolet light. High concentrations of tropospheric O_3 not only
68 pose a threat to human health but also harm agricultural crops and other aspects of the
69 ecosystem (Lippmann, 1989; West et al., 2006; Xiao et al., 2021; Feng et al., 2022).
70 Despite the strict emission reduction measures implemented since the so called
71 “National Ten Measures” (Air Pollution Prevention and Control Action Plan, 2012-
72 2017) and the “Blue Sky Protection Campaign” (2017-2020) in China, O_3 pollution has
73 been rapidly increasing and spreading across larger areas, becoming the primary
74 pollutant in many regions of China (Wang et al., 2017; Lu et al., 2018; Wang et al.,
75 2019; Lyu et al., 2023).

76 Current research on O_3 pollution in China primarily focuses on anthropogenic
77 emissions, with limited attention given to natural sources, such as biogenic volatile
78 organic compounds (BVOCs). BVOCs are highly reactive and, once released, rapidly
79 interact with atmospheric oxidants such as hydroxyl radicals (OH), leading to increased
80 concentrations of O_3 and other oxidative products. (Jenkin and Clemitshaw, 2000; Fry
81 et al., 2014; Cao et al., 2022; Gao et al., 2022; Wang et al., 2022b). In urban
82 environments with high nitrogen oxide levels, O_3 formation is particularly sensitive to
83 VOCs, meaning that even low concentrations of BVOCs can significantly impact O_3
84 levels. For instance, BVOC emissions from urban greening spaces, in combination with
85 anthropogenic emissions, can contribute to an additional increase of approximately 5
86 ppb in O_3 concentrations in Beijing (Ma et al., 2019). Likewise, the intermediate
87 oxidation products of BVOCs, such as methyl vinyl ketone (MVK) and methacrolein
88 (MAC) from South China’s forests, can interact with anthropogenic emissions from the
89 Yangtze River Delta (YRD) and Pearl River Delta (PRD) urban clusters through
90 regional transport, leading to elevated O_3 levels in downstream cities (Wang et al.,
91 2022b).

92 It is important that the BVOC emissions, particularly isoprene emissions, are closely



93 related to meteorological conditions. Typically, isoprene emissions increase with rising
94 temperatures (or solar radiation); however, when temperatures become too high,
95 vegetation growth is inhibited, and isoprene emissions may decrease due to stomata
96 close (Seco et al., 2022). Recent research has found that under mild to moderate heat
97 stress, reduced stomatal conductance in vegetation leads to increased leaf temperatures,
98 which can indirectly enhance isoprene emissions from plants (Wang et al., 2022a).
99 Numerous studies have found that synoptic weather systems with high temperatures
100 significantly exacerbate BVOC emissions from vegetation. For instance, several studies
101 have report that the rare heatwave during the summer of 2022 exacerbated O₃ pollution
102 by intensifying BVOC emissions in the YRD, PRD and Sichuan Basin regions (Li et
103 al., 2024; Wang et al., 2024b; Wang et al., 2024a).

104 The Pearl River Delta (PRD) is a typical developed urban cluster located in southern
105 China. This region is characterized by distinct geographical features: urban areas are
106 characterized by high levels of anthropogenic emissions, while the surrounding areas
107 are densely vegetated. Due to climate change and ongoing greening efforts, vegetation
108 in this region has significantly increased, particularly the evergreen broadleaf forests,
109 which are known for their high BVOC emissions. (Guenther et al., 2006; Guenther et
110 al., 2012; Wang et al., 2023). Currently, air quality issues in the PRD have shifted from
111 PM_{2.5}-dominated haze pollution to O₃-dominated photochemical pollution. A
112 substantial amount of research has been conducted on the characteristics of O₃ pollution.
113 For example, Yin et al. (2019) found that summer O₃ concentrations in the region are
114 relatively low due to monsoon influence, with higher values observed in autumn; Jin
115 and Holloway (2015) discovered seasonal variations in the sensitivity of O₃ to its
116 precursors, indicating that the cold season is VOCs-limited, while summer often
117 exhibits a NO_x-limited or synergistic control regime. However, past studies have
118 primarily focused on the impact of anthropogenic emissions, with limited attention
119 given to the effects of natural sources. The impact of increased natural emissions from
120 vegetation and climate warming on local O₃ levels remains unclear.

121 In this study, we combined comprehensive observations to analyze the summer O₃ and



122 vegetation trends in the PRD region. Using a dynamic MEGAN model for biogenic
123 emissions, we quantified the changes in BVOC emissions caused by vegetation and
124 climate change, and the meteorological factors driving these BVOC changes were also
125 identified. Finally, we would assess the impact of BVOC variations and anthropogenic
126 emission reductions on O₃ levels. This study aims to provide scientific insights into the
127 mechanisms of O₃ pollution and emphasize the importance of control strategies that
128 account for the synergistic effects of both anthropogenic and natural emissions in the
129 context of climate warming.

130 **2. Material and Methods**

131 **2.1 Data**

132 We integrated surface O₃ observations with O₃ sounding data to investigate the
133 spatiotemporal variations of O₃ in the Pearl River Delta (PRD) region. The surface O₃
134 data were sourced from the monitoring network established by China's Ministry of
135 Ecology and Environment (MEE), comprising 89 operational stations across the PRD
136 (Fig. 1). These networks provide in-situ observations of ambient hourly O₃, CO, SO₂,
137 NO₂, PM_{2.5} and PM₁₀ concentrations after 2013. In addition, complementary O₃
138 sounding data were sampled at King's Park, Hong Kong (114.17° N, 22.31° E), where
139 operational O₃ sounding has been conducted since 1993. Soundings are performed
140 weekly at 14:00 local time using balloons, providing vertical profiles with a resolution
141 of approximately 10 m, reaching altitudes of up to ~30 km. In this study, we collected
142 O₃ soundings from the surface up to 900 hPa (within the boundary layer) to represent
143 the background O₃ levels in the PRD region.

144 In order to understand the nitrogen oxides (NO_x), a precursor of O₃, satellite
145 observations and emission inventory were analyzed. Monthly tropospheric NO_x
146 column data (Level 3) were obtained from the OMI satellite instrument (data accessed
147 via: <https://avdc.gsfc.nasa.gov/pub/data/satellite/Aura/OMI>, last access Aug 20, 2024).
148 Anthropogenic NO_x emissions were derived from the Multi-resolution Emission
149 Inventory for China (MEIC) developed by Tsinghua University
150 (<https://meicmodel.org.cn/>, last access Aug 20, 2024).



151 **2.2 MEGAN model**

152 Biogenic emissions were computed offline using the Model of Emissions of Gases and
153 Aerosols from Nature version 2.1 (MEGAN) developed by Guenther et al. (2012).
154 MEGAN model is capable of estimating the emissions of over a hundred biogenic
155 volatile organic compounds (BVOCs), with a horizontal resolution that can range from
156 ~ 500 meters to hundreds of kilometers. The theoretical calculations are based on the
157 following concept:

$$F_i = \gamma_i \sum \varepsilon_{ij} \chi_j \quad (1)$$

158 where F_i , ε_{ij} and χ_j are emission amount, standard emission factor and fractional
159 coverage of each plant functional type (PFT) j of chemical species i . γ_i is the emission
160 activity factor, which is calculated based on canopy environment coefficient (C_{CE}), leaf
161 area index (LAI), light (γ_L), temperature (γ_T), leaf age (γ_{LAI}), soil moisture (γ_{SM}), and
162 CO_2 uptake (γ_{CI}):

$$\gamma_i = C_{CE} LAI \gamma_{L,i} \gamma_{T,i} \gamma_{LAI,i} \gamma_{SM,i} \gamma_{CI,i} \quad (2)$$

163 In China, most researchers using MEGAN rely on the model's default surface data.
164 However, this default data is based on conditions from the year 2000, with no annual
165 variation. Considering the significant changes in land cover due to China's reforestation
166 policies and climate change, the outdated land surface data fails to capture current
167 conditions accurately. Therefore, this study employs satellite-derived, high-resolution
168 land data with monthly dynamic updates to achieve more representative and accurate
169 estimates of BVOC emissions. In detail, the LAI data are sourced from the MODIS
170 MCD15A2H product covering the period from 2001 to 2020, with a temporal resolution
171 of 8 days. The land cover type data are derived from the MODIS MCD12Q1 product,
172 which uses an LAI-based classification scheme and includes 8 vegetation types. These
173 were further mapped to the 16 plant functional types (PFTs) used in MEGANv2.1 with
174 the consideration of the methodology outlined by Bonan et al. (2002) The detailed
175 mapping scheme were provided in the supplementary (Table S1). Meteorological
176 conditions were provided by Weather Research and Forecasting (WRF) simulations.
177 Using this method, we were capable to separately quantify the impact of vegetation



178 emissions driven by changes in vegetation distribution and those driven by climate
179 change. For instance, by fixing the meteorological conditions while allowing the
180 vegetation data to change annually, we could isolate the contribution of vegetation
181 distribution variations to emissions (land impact). Similarly, by holding the vegetation
182 data constant and allowing meteorological conditions to vary year by year, the
183 emissions attributable to climate change could be quantified (climate impact).

184 **2.3 Random Forest model**

185 To investigate the relationship between BVOC emissions and meteorological factors,
186 we employed a Random Forest (RF) machine learning model. Since BVOC emissions
187 were calculated based on the MEGAN-calculation framework, where emissions are
188 driven by inputs such as temperature, humidity, solar radiation and etc. This context
189 makes the RF model particularly suitable, as it is adept at handling non-linear
190 relationships and interactions among variables, making it effective for complex
191 environmental datasets. We trained the RF model using the WRF simulated
192 meteorological variables alongside corresponding BVOC emission. To interpret the
193 results and gain insights into the contribution of each meteorological factor to BVOC
194 emissions, we utilized Shapley Additive Explanations (SHAP) values. SHAP values
195 provide a robust framework for understanding the impact of individual features on
196 model predictions by attributing the contribution of each factor to the overall output.
197 This approach not only enhances the interpretability of the RF model but also facilitates
198 a deeper understanding of how different meteorological conditions influence BVOC
199 emissions, thereby informing future research and environmental management strategies.

200 **2.4 WRF-CMAQ model**

201 We employed the WRF-CMAQ (Weather Research and Forecasting-Community
202 Multiscale Air Quality) chemical transport model to assess the effects of climate and
203 land-change-induced BVOC emissions, alongside anthropogenic emission reductions,
204 on O₃ concentrations. The WRF mode (version 3.9.1) is a mesoscale numerical weather
205 prediction system designed for both operational forecasting and atmospheric research.
206 Atmospheric chemistry was simulated using CMAQ (version 5.3), with the Carbon



207 Bond version 06 (CB06) and Aerosol Module version 6 (AERO6) mechanism. In this
208 study, we utilized a single domain with a horizontal resolution of 25 km, covering the
209 entirety of China and its surrounding regions, centered at 30°N, 106.8°E. The model
210 includes 31 vertical layers with a top pressure boundary of 100 hPa. The WRF model
211 was driven by ERA5 reanalysis data, providing meteorological inputs for the simulation.
212 The chemical boundary conditions for the CMAQ domain were sourced from the
213 Community Earth System Model (CESM).
214 The key WRF-CMAQ configurations include the Rapid Radiative Transfer Model
215 (RRTM) for longwave and shortwave radiation, the Noah Land Surface Model for land-
216 atmosphere interactions, the Kain-Fritsch scheme for cumulus parameterization, the
217 Lin microphysics scheme, and the YSU boundary layer scheme. Anthropogenic
218 emissions for China were obtained from the Multi-resolution Emission Inventory for
219 China (MEIC), and biogenic emissions were calculated by the improved MEGAN
220 model (described in Section 2.2). The performance of the model was validated by
221 comparing with observations. Generally, the statistical comparisons showed that the
222 model simulated results matched well with those observed, indicating a reliable model
223 performance (summarized in Table S2).
224 Using the WRF-CMAQ model, we conducted parallel comparison experiments to
225 address the importance of BVOCs emissions. For example, scenarios that consider only
226 anthropogenic emissions (AVOC_Only) versus those that include both anthropogenic
227 and vegetation emissions (Add_BVOC). To explore the complex nonlinear
228 relationships between O₃ and its precursors, we employed the HDDM (High-order
229 Decoupled Direct Method) approach. In HDDM, sensitivity coefficients (S_j) represent
230 the response of a chemical concentration to perturbations in a sensitivity parameter,
231 such as emissions, initial conditions, boundary conditions, or reaction rates (Simon et
232 al., 2013; Itahashi et al., 2015). The semi normalized first- and second-order sensitivity
233 coefficients, $S_j^{(1)}$ and $S_{j,k}^{(2)}$ are defined as follows,

$$S_j^{(1)} = \frac{\partial C}{\partial E_j} \quad (3)$$



$$S_{j,k}^{(2)} = \frac{\partial^2 C}{\partial E_j \partial E_k} \quad (4)$$

234 , where $S_j^{(1)}$ represents the first-order sensitivity to changes in parameter j . $S_{j,k}^{(2)}$ refers
 235 to the second-order sensitivity to simultaneous changes in parameter j and k . When $j=k$,
 236 $S_{j,j}^{(2)}$ means the sensitivity to an individual parameter, and when $j \neq k$, it refers to a cross-
 237 sensitivity coefficient. The equation for approximating O_3 concentrations under the
 238 perturbations of parameters j and k through a Taylor-series expansion of the sensitivity
 239 coefficients is as follows:

$$C_{(\Delta E_j, \Delta E_k)} = C_0 + S_j^{(1)} \Delta E_j + \frac{1}{2} S_j^{(2)} \Delta E_j^2 + S_k^{(1)} \Delta E_k + \frac{1}{2} S_k^{(2)} \Delta E_k^2 + \Delta E_j \quad (5)$$

$$\Delta E_k S_{j,k}^{(2)}$$

240 , where C_0 refers to the chemical concentration in the base scenario.

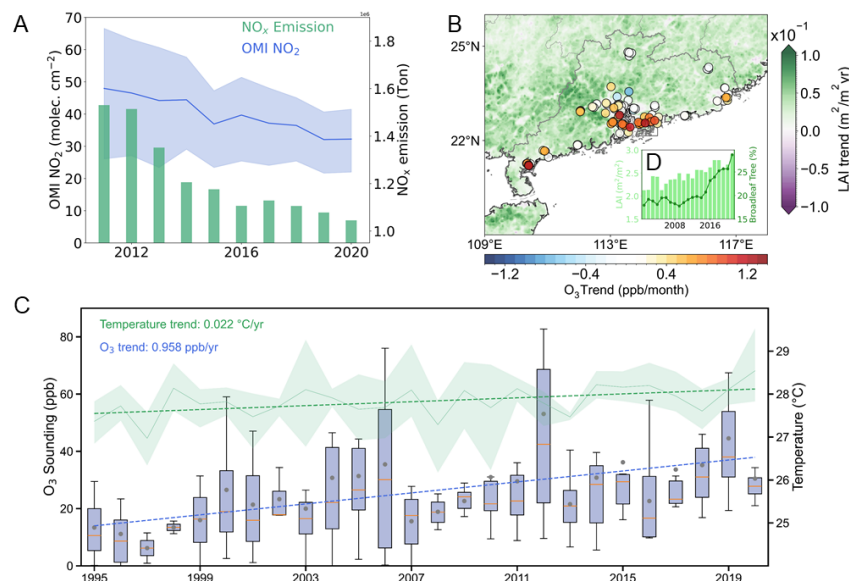
241 Besides, O_3 formation budget based on the perspectives of anthropogenic emission
 242 reductions and changes in vegetation emissions were quantified over the last decades
 243 (2001-2020). This algorithm maximally accounts for the influences of various
 244 processes to highlight their respective contributions. For instance, anthropogenic NOx
 245 emissions peaked in 2012 and have continuously declined over the past decade.
 246 Therefore, we assessed the impact of human emission reductions by comparing O_3
 247 simulations driven by emissions from 2012 and 2020. Similarly, considering the
 248 continuous increase in surface vegetation data, we utilized surface vegetation data from
 249 2001 and 2020 to drive the vegetation emissions aiming to maximize the differences in
 250 O_3 simulations resulting from changes in vegetation. To account for the impact of
 251 climate change-driven vegetation emissions, we calculated BVOC emissions using both
 252 current and historical meteorological data. We then examined the differences in O_3
 253 simulations driven by current and past meteorological data. The impact of climate-
 254 driven meteorology on chemical O_3 formation could also be identified using similar
 255 methods (see details in Table S3). Although this algorithm does not operate within a
 256 unified time frame, it emphasizes the contributions of both anthropogenic and
 257 vegetation emissions, aiding in the assessment of their combined effects.

258



259 **3 Results**

260 **3.1 Rising summer O₃ concentrations and vegetation in PRD**



261

262 Figure 1 (A) Changes of tropospheric NO₂ column concentrations and anthropogenic NO_x emissions in PRD from
 263 2011 to 2020. (B) PRD map showing surface observed summer O₃ trends (2013-2020) and leaf area index
 264 (LAI, 2001-2020). (C) Changes of LAI and proportion of broad leaf trees in PRD between 2001 and 2020. (D)
 265 Variation of summer O₃ soundings and temperature, the dashed lines were the linear plot.

266 Since China implemented the "National Ten Measures" in 2012, aimed at controlling
 267 PM_{2.5} pollution, NO_x emissions have shown significant improvement in PRD, as
 268 evidenced by the substantial annual decline in NO_x column density and emissions from
 269 2011 to 2020 (Fig. 1A). However, surface monitoring summer O₃ concentrations in the
 270 PRD region exhibited an upward trend with an increasing rate of 0.51 ppb/month (Fig.
 271 1B). We also examined background O₃ sounding data within the boundary layer
 272 (between surface and 900hPa), the results revealed an increasing rate of 0.96 ppb/year
 273 between 1995 and 2020, consistent with the surface network observation (Fig. 1C). It
 274 has been widely acknowledged that summer O₃ levels in the PRD are generally low due
 275 to the monsoon-prevailing southerly winds, which brings relatively clean air from
 276 South China Sea. However, the rising O₃ concentrations in recent summers suggest that
 277 photochemical O₃ pollution is becoming increasingly severe in the PRD.



278 Driven by the government’s reforestation policies and the impact of climate change, we
279 also observed an increasing trend in vegetation coverage in the PRD, as indicated by
280 the broad positive LAI trend over the last two decades (Fig. 1B). Additionally, through
281 the analysis of changes in vegetation types, it was found a significant increase in the
282 proportion of evergreen broadleaf forests, a tree type known for high BVOC emissions,
283 rising from 17.9% to 28.6% between 2010 and 2020 in PRD (Fig. 1D). The increase of
284 the vegetation coverage implies a potential rise in BVOC emissions, which appears to
285 be a possible contributor to the observed O₃ increment. Additionally, against the
286 backdrop of global climate warming, the PRD has experienced a temperature increase
287 of +0.02°C/year over the past decade (Fig. 1C), which would further enhance BVOC
288 emissions due to elevated temperatures.

289 3.2 Significant BVOC emission increment due to climate change

290

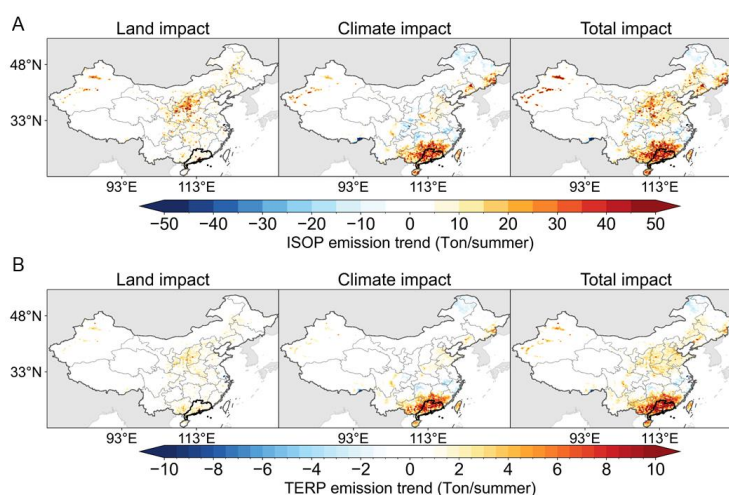
Table 1 Comparisons of Isoprene emissions and their proportion of total BVOCs.

Isoprene emission (Tg)	Isoprene/BVOCs (%)	Reference
17.5	53.9	This study
15.94	46.5	Wang et al. (2021a)
9.6	50	Cao et al. (2018)
9.59	50.9	Fu and Liao (2012)
13.3	56.5	Wu et al. (2020)
15	52.8	Guenther et al. (1995)
19.13-27.09	52.4	Li and Xie (2014)
20.7	42.5	Li et al. (2013)
28.23-37.45	57.6-63.6	Li et al. (2020)

291 As detailed in the methods section, we updated the MEGAN model by incorporating
292 dynamically varying satellite-derived vegetation data. To assess the model's reliability,
293 we calculated the BVOC emissions for the entire year of 2020 in China, utilizing 2020-
294 based meteorology and land data, and compared the findings with results from
295 previously published studies (Table 1). The BVOC inventory established in this study



296 indicates that total isoprene emissions in China reached 17.5 Tg, falling within mid-
297 range estimates from previous studies (Table 1), suggesting overall consistency with
298 earlier findings. Notably, isoprene accounts for 53.9% of all BVOC emissions, a
299 proportion that also aligns well with earlier findings. This not only supports the validity
300 of our calculations but also underscores the significance of isoprene across all BVOC
301 species.



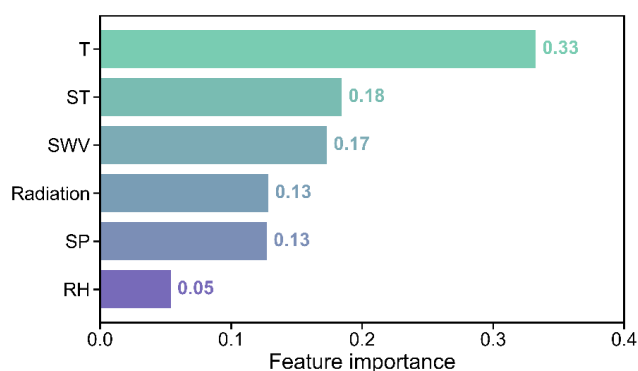
302

303 Figure 2. Summer isoprene (A) and terpene (B) emission trend in mainland China between 2001 and 2020. The
304 land impact refers to BVOCs emissions (ISOP for isoprene, TERP for terpene) from vegetation cover change,
305 while the climate impact refers to BVOCs emissions due to climate change. The black line in the map highlights
306 the administrative boundary of the PRD region.

307 By using different combinations of meteorological conditions and land cover data
308 (including LAI and PFT), we employed the MEGAN model to quantify the impact of
309 land use and climate changes on BVOC emission trends from 2001 to 2020,
310 respectively. The two major components of BVOCs, isoprene and terpenes, were both
311 quantified in response to changes in vegetation cover and climate. Our findings indicate
312 a significant upward trend in both isoprene and terpene emissions in southern China
313 (including PRD) and northern China, which stand in stark spatial contrast to the
314 emissions patterns observed in western and central China. By attributing the emission
315 changes to vegetation and climate shifts, we found that, unlike northern regions of
316 China, such as the Loess Plateau, where increased BVOC emissions are primarily



317 attributed to afforestation efforts (Zhang et al., 2016), the rise in BVOC emissions in
318 southern China is mainly influenced by climate change. For example, the isoprene
319 emission trend was 30.0 Ton/summer over 2001-2020 in PRD, taking up ~ 80% total
320 isoprene variations. The significant increase attributed to climate change suggests that
321 BVOC emissions in this area are highly sensitive to climatic variations.



322

323

Figure 3. Feature importance of meteorological parameter on BVOCs emissions

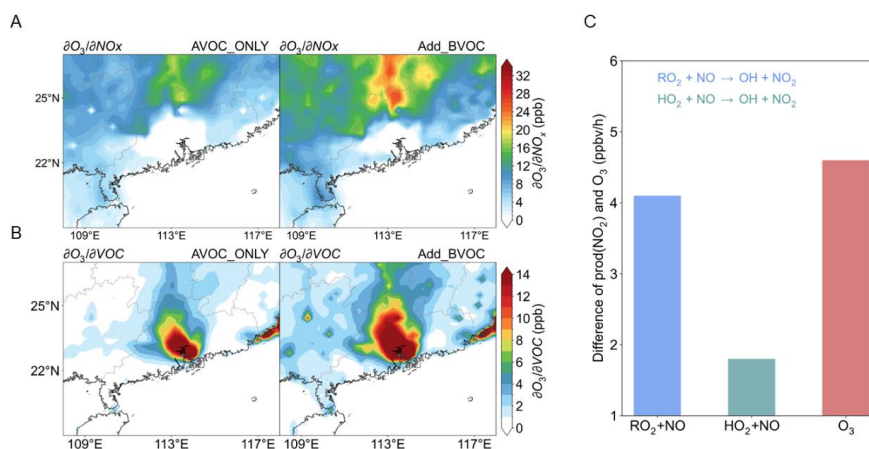
324 The climate impact could be simply attributed to the combined effects of multiple
325 meteorological parameters, such as ambient temperature, soil temperature, relatively
326 humidity and so on. It is crucial to identify the dominant meteorological factors under
327 the context of climate warming. To this end, we established a diagnostic method that
328 coupled numerical model with machine learning. Specifically, we utilized
329 meteorological parameters simulated by the WRF model to drive a Random Forest (RF)
330 model aimed at training BVOCs emissions. To assess the significance of each
331 meteorological parameter, we employed the SHAP (SHapley Additive exPlanations)
332 method (see details in methods). The results indicated that ambient temperature, soil
333 temperature, soil water vapor, radiation, surface pressure, and relative humidity are the
334 dominant meteorological parameters, with temperature being the most influential. This
335 finding is further supported by the observed upward trend in these parameters over the
336 past 20 years (Fig S1). Our investigation reveals that BVOC emissions in PRD are
337 highly sensitive to the climate and the rising temperature has become the dominant
338 factor driving the increase in BVOC emissions. Noting that the PRD is a developed city



339 clusters with high anthropogenic emissions, the annual rise in BVOC emissions is likely
 340 to exacerbate the interactions between natural and human-made emissions. Therefore,
 341 the impact of BVOCs emissions warrants further exploration in addressing the issue of
 342 increasing summer O₃ levels in the region.

343 3.3 Climate induced BVOC alleviates O₃ control

344 To quantify the influence of BVOC on O₃ concentrations, the CMAQ-HDDM model
 345 was employed to assess the sensitivity of O₃ to its precursors during the summer of
 346 2020 in southern China. The response of atmospheric oxidation capacity to BVOC
 347 emissions was evaluated under two scenarios: one considering only the impact of
 348 anthropogenic VOCs (AVOC_ONLY scenario), and the other accounting for both
 349 anthropogenic and biogenic emissions (ADD_BVOC scenario). Noting that the
 350 AVOC_ONLY scenario is an unrealistic scenario and removing BVOCs emissions from
 351 the real-world may result in uncertainties due to the non-linear relationship between O₃
 352 and its precursors, however, studying and comparing the parallel numerical experiments
 353 (AVOC_ONLY and ADD_BVOC scenarios) could greatly help us understand the
 354 mechanisms and significance of BVOC emissions on O₃ formation. In each scenario,
 355 we primarily focused on the responses of O₃ to NO_x emission reductions, aligning with
 356 China's emission control strategy that predominantly targets NO_x emissions.



357
 358 Figure 4. (A) Spatial distribution of O₃ sensitivity coefficients to NO_x emissions under AVOC_ONLY and
 359 Add_BVOC scenario. (B) Same as (A) but for sensitivity coefficients to VOCs emissions. (C) difference of



360 production rate of NO₂ (via chemical pathway of RO₂+NO and HO₂+NO) and O₃ at 14:00 between AVOC_ONLY
361 and Add_BVOC scenario

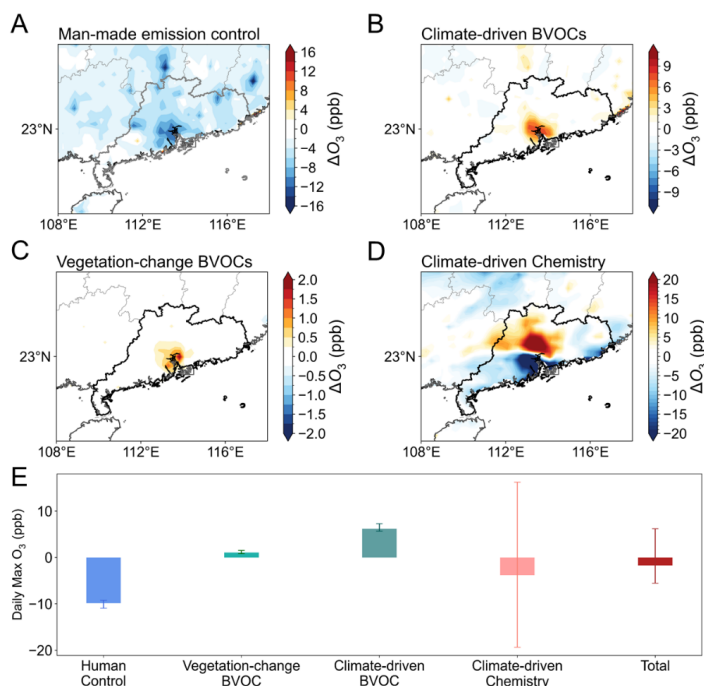
362 Taking the 2020-based simulation as an example, we analyzed the spatial distribution
363 of the first-order sensitivity coefficient of O₃ to its precursors (Fig. 4A-B). Under the
364 AVOC_ONLY scenario, the central region of the PRD exhibited significant sensitivity
365 to VOC emissions (i.e., high sensitivity coefficients were over 15 ppb), while the
366 surrounding areas were more NO_x-sensitive (Fig. 4A). When BVOC emissions were
367 included, the VOC-sensitive region expanded beyond the core of the PRD to its
368 surrounding areas, also with an increase in the sensitivity coefficient value. This implied
369 that a more favorable condition for O₃ production. Additionally, in remote areas that
370 belonged to NO_x-sensitive, for instance the northern PRD, a notable increase of the
371 sensitivity coefficient value was found, meaning the sensitivity of O₃ to NO_x emissions
372 also became more pronounced (Fig. 4B). This suggests that even in NO_x-limited regions,
373 BVOCs could significantly enhance atmospheric reactivity, facilitating easier O₃
374 formation. The underlying mechanism by which BVOC emissions influence ozone
375 formation can be attributed to their impact on NO₂ production levels (Fig. 4C). By
376 comparing the reaction rates of RO₂ + NO and HO₂ + NO, both key pathways
377 determining O₃ formation, we found that the addition of BVOCs increased these
378 reaction rates by 4.1 ppb/h and 1.8 ppb/h, respectively. In other words, the presence of
379 BVOCs enhanced atmospheric oxidizing capacity, leading to an additional O₃
380 production rate of approximately 4.7 ppb/h. Further, we simulated O₃ responses to NO_x
381 emission perturbations under both scenarios (Fig. S2). The result showed that O₃ levels
382 initially rose and then fall as NO_x reductions increased, with a turning point around a
383 10% emission reduction. Compared to our previous study conducted in winter, which
384 identified the O₃ formation regime as transition-limited with a turning point at
385 approximately 35% NO_x emission reduction (Wang et al., 2021b), it is believed that O₃
386 formation sensitivity in the PRD during summer is more closely aligned with a NO_x-
387 limited regime. However, after considering the influence of BVOC emissions, the
388 benefits of NO_x reduction were offset by the influence of BVOC emissions, which
389 contributed an additional ~ 5 ppb of O₃ formation.



390 Next, leveraging scenario simulations with the CMAQ model, we quantified the O₃
391 formation budget from the perspectives of anthropogenic emission reductions and
392 changes in vegetation emissions over the past decades (Fig. 5). Despite the
393 implementation of China's "Ten Measures" (2012-2017) and the "Blue Sky Protection
394 Campaign" (2017-2020) pollution control strategies, observational data have shown a
395 rise in O₃ levels, which contradicts expectations and has puzzled policymakers in
396 formulating effective O₃ control strategies. However, when considering only
397 anthropogenic emissions (AVOC_ONLY scenario), emission reductions could lead to
398 varying degrees of O₃ decline in southern China. For example, the average O₃
399 concentrations in Guangzhou could potentially decrease by 9.8 ppb due to man-made
400 emission control (Fig. 5A). This was an outcome that government regulators would be
401 pleased to see. However, the "benefit" has been overshadowed by the increase in BVOC
402 emissions (ADD_BVOC scenario). Our research indicated that the key driver of rising
403 summer O₃ levels was the significant impact of BVOC emissions. Specifically, BVOC
404 emissions driven by climate warming significantly impacted O₃ concentrations,
405 showing a pronounced positive effect in the core of the PRD urban areas (Fig. 5B). In
406 Guangzhou, climate-driven BVOC emissions have contributed to an increase in O₃
407 levels by as much as 6.2 ppb. In comparison, BVOC emissions resulting from
408 vegetation distribution variations (vegetation-change BVOC) contributed less to O₃
409 formation, but still had a positive impact, with a contribution ranging from 0.8 to 1.5
410 ppb. It is noteworthy that the contribution of climate impact on O₃ chemistry (Climate-
411 driven chemistry) varied significantly, with values ranging from -19.3 to 16.2 ppb. This
412 substantial difference might be attributed to perturbations caused by extreme weather
413 events. For instance, extreme stable weather conditions, such as heatwaves, are
414 conducive to O₃ pollution, while intense heavy rainfall facilitates O₃ removal. Indeed,
415 the PRD is highly susceptible to extreme weather events during the summer, such as
416 the periphery of typhoons (heatwaves) and strong rainfall brought by squall lines. As
417 an overall effect, BVOC emissions have undermined or offset the progress achieved
418 through anthropogenic emission controls, leading to only marginal reductions or, in



419 some cases, even increases in O₃ concentrations (Fig. 5E).



420

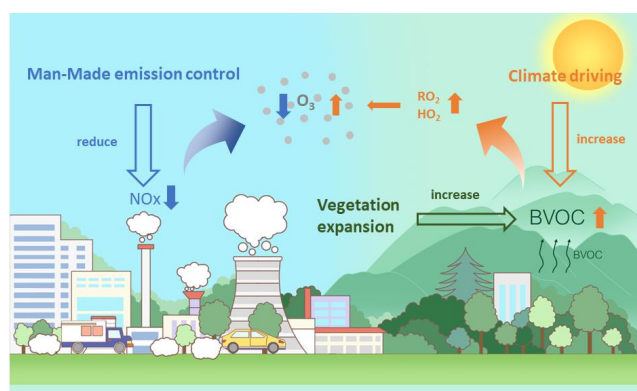
421 Figure 5. Impact of O₃ formation based on a maximal account for the influence of (A) man-made emission control,
 422 (B) climate-driven BVOC emissions, (C) vegetation-change BVOC, and (D) climate-driven meteorology on
 423 chemistry in the PRD region. (E) Daily max O₃ budget in Guangzhou city.

424 4. Conclusion and Implication

425 Due to the influence of the summer monsoon, O₃ concentrations in the PRD during
 426 summer are typically low and often overlooked. However, observational data indicates
 427 a rising trend in summer O₃ levels over the past decades, with an increase of
 428 approximately 1 ppb per summer. Based on the current understanding of O₃ formation
 429 sensitivity, it is widely acknowledged that the O₃ formation regime in the PRD tends to
 430 exhibit either a transitional or NO_x-limited regime during summer. (Jin and Holloway,
 431 2015; Wang et al., 2019). China's emphasis on reducing nitrogen oxide emissions over
 432 the past decade is expected to have contributed to lower summer O₃ levels. In response
 433 to the unexpected rise in summer O₃, our dynamically calculated natural emissions
 434 reveal a significant increase in BVOC emissions in the region between 2001 and 2020.



435 This increase was primarily driven by climate change and changes in vegetation cover,
436 with climate-driven BVOC emissions accounting for approximately 80% of the rise.
437 The concurrent increase in atmospheric and soil temperatures emerged as the key
438 factors driving this increase in BVOC emissions. Based on parallel numerical
439 simulations using the WRF-CMAQ models, we found that vegetation emissions driven
440 by climate warming have mitigated, and in some cases even offset, the effects of
441 anthropogenic emission reductions, serving as a key factor in the unexpected rise of O₃
442 levels in the PRD (Fig. 6).



443
444 Figure 6. The conceptual scheme illustrating how climate-driven BVOCs emissions alleviate or offset man-made
445 emission control against O₃.

446 China has proposed its ambitious strategies for carbon peaking and carbon neutrality,
447 and for sure, will continue to enhance its efforts to reduce anthropogenic emissions. In
448 the context of global warming, rising temperatures and carbon neutrality-induced
449 greening are likely to enhance biogenic emissions, underscoring the increasing
450 importance of natural sources in urban areas. Our findings highlight the significant role
451 of climate-induced natural sources in tropospheric O₃ formation, even in regions with
452 high anthropogenic activity, and emphasize the importance of mitigating climate
453 warming. Lastly, it is recommended that future pollution control strategies shall take
454 into account the synergistic effects of both anthropogenic and natural sources.

455

456



457

458 **Acknowledgments**

459 This research is supported by the National Key Research and Development Program
460 (grant no. 2023YFC3709304), the National Natural Science Foundation Major Project
461 (grant no. 42293322), the Youth Fund Project of the Sichuan Provincial Natural Science
462 Foundation (24NSFSC2988), the special found of State Environmental Protection Key
463 Laboratory of Formation and Prevention of Urban Air Pollution Complex (SEPAir-
464 2024080211), the Guangdong Basic and Applied Basic Research Foundation (Grant No.
465 2022A1515011753) and the Fundamental Research Funds for the Central Universities
466 (Grant No. YJ202313). The authors also thank the Tsinghua University for developing
467 and sharing the MEIC emission inventory.

468

469 **Data Availability Statement**

470 Air pollutant data was collected through dynamic web scraping from the Environmental
471 Monitoring Station of China: <https://air.cnemc.cn:18007/>. The O₃ sounding data at
472 Hong Kong could be downloaded from: <https://woudc.org/data/explore.php>.
473 Meteorological data from ERA5 are available at:
474 <https://cds.climate.copernicus.eu/datasets>. The MODIS land data is from:
475 <https://e4ftl01.cr.usgs.gov/MOTA/>. The numerical simulation results were stored in
476 Tianhe-2 supercomputer, and results could be acquired from Dr. Nan Wang
477 (nan.wang@scu.edu.cn)

478

479 **Author Contributions**

480 N.W. and H.L. designed the research. N.W. conducted the simulation and wrote the
481 manuscript. N.W., H.L., W.X., and S.L. contributed to the interpretation of the results.
482 All the authors provided critical feedback and helped to improve the manuscript.

483

484 **Competing Interests**

485 The authors declare that they have no known competing financial interests
486 or personal relationships that could have appeared to influence the work.

487

488



489 **Primary Sources**

490 **Secondary Sources**

491 **Uncategorized References**

492 Bonan, G. B., Levis, S., Kergoat, L., and Oleson, K. W.: Landscapes as patches of plant functional
493 types: An integrating concept for climate and ecosystem models, *Global Biogeochemical Cycles*,
494 16, 5-1-5-23, 2002.

495 Cao, H., Fu, T.-M., Zhang, L., Henze, D. K., Miller, C. C., Lerot, C., Abad, G. G., De Smedt, I., Zhang,
496 Q., and van Roozendaal, M.: Adjoint inversion of Chinese non-methane volatile organic compound
497 emissions using space-based observations of formaldehyde and glyoxal, *Atmospheric Chemistry
498 and Physics*, 18, 15017-15046, 2018.

499 Cao, J., Situ, S., Hao, Y., Xie, S., and Li, L.: Enhanced summertime ozone and SOA from biogenic
500 volatile organic compound (BVOC) emissions due to vegetation biomass variability during 1981–
501 2018 in China, *Atmospheric Chemistry and Physics*, 22, 2351-2364, 2022.

502 Feng, Z., Xu, Y., Kobayashi, K., Dai, L., Zhang, T., Agathokleous, E., Calatayud, V., Paoletti, E.,
503 Mukherjee, A., and Agrawal, M.: Ozone pollution threatens the production of major staple crops
504 in East Asia, *Nature Food*, 3, 47-56, 2022.

505 Fry, J. L., Draper, D. C., Barsanti, K. C., Smith, J. N., Ortega, J., Winkler, P. M., Lawler, M. J., Brown, S.
506 S., Edwards, P. M., and Cohen, R. C.: Secondary organic aerosol formation and organic nitrate yield
507 from NO₃ oxidation of biogenic hydrocarbons, *Environmental science & technology*, 48, 11944-
508 11953, 2014.

509 Fu, Y. and Liao, H.: Simulation of the interannual variations of biogenic emissions of volatile organic
510 compounds in China: Impacts on tropospheric ozone and secondary organic aerosol, *Atmospheric
511 Environment*, 59, 170-185, 2012.

512 Gao, Y., Ma, M., Yan, F., Su, H., Wang, S., Liao, H., Zhao, B., Wang, X., Sun, Y., and Hopkins, J. R.:
513 Impacts of biogenic emissions from urban landscapes on summer ozone and secondary organic
514 aerosol formation in megacities, *Science of the Total Environment*, 814, 152654, 2022.

515 Guenther, A., Karl, T., Harley, P., Wiedinmyer, C., Palmer, P. I., and Geron, C.: Estimates of global
516 terrestrial isoprene emissions using MEGAN (Model of Emissions of Gases and Aerosols from
517 Nature), *Atmospheric Chemistry and Physics*, 6, 3181-3210, 2006.

518 Guenther, A., Jiang, X., Heald, C. L., Sakulyanontvittaya, T., Duhl, T. a., Emmons, L., and Wang, X.:
519 The Model of Emissions of Gases and Aerosols from Nature version 2.1 (MEGAN2. 1): an extended
520 and updated framework for modeling biogenic emissions, *Geoscientific Model Development*, 5,
521 1471-1492, 2012.

522 Guenther, A., Hewitt, C. N., Erickson, D., Fall, R., Geron, C., Graedel, T., Harley, P., Klinger, L., Lerdau,
523 M., McKay, W. A., Pierce, T., Scholes, B., Steinbrecher, R., Tallamraju, R., Taylor, J., and Zimmerman,
524 P.: A global model of natural volatile organic compound emissions, *Journal of Geophysical
525 Research: Atmospheres*, 100, 8873-8892, 10.1029/94JD02950, 1995.

526 Itahashi, S., Hayami, H., and Uno, I.: Comprehensive study of emission source contributions for
527 tropospheric ozone formation over East Asia, *Journal of Geophysical Research: Atmospheres*, 120,
528 331-358, 2015.

529 Jenkin, M. E. and Clemitshaw, K. C.: Ozone and other secondary photochemical pollutants:
530 chemical processes governing their formation in the planetary boundary layer, *Atmospheric
531 Environment*, 34, 2499-2527, 2000.



- 532 Jin, X. and Holloway, T.: Spatial and temporal variability of ozone sensitivity over China observed
533 from the Ozone Monitoring Instrument, *Journal of Geophysical Research: Atmospheres*, 120,
534 7229-7246, 2015.
- 535 Li, L. and Xie, S.: Historical variations of biogenic volatile organic compound emission inventories
536 in China, 1981–2003, *Atmospheric environment*, 95, 185-196, 2014.
- 537 Li, L., Chen, Y., and Xie, S.: Spatio-temporal variation of biogenic volatile organic compounds
538 emissions in China, *Environmental pollution*, 182, 157-168, 2013.
- 539 Li, L., Yang, W., Xie, S., and Wu, Y.: Estimations and uncertainty of biogenic volatile organic
540 compound emission inventory in China for 2008–2018, *Science of the Total Environment*, 733,
541 139301, 2020.
- 542 Li, M., Huang, X., Yan, D., Lai, S., Zhang, Z., Zhu, L., Lu, Y., Jiang, X., Wang, N., and Wang, T.: Coping
543 with the concurrent heatwaves and ozone extremes in China under a warming climate, *Science
544 Bulletin*, 2024.
- 545 Lippmann, M.: Health effects of ozone a critical review, *Japca*, 39, 672-695, 1989.
- 546 Lu, X., Hong, J., Zhang, L., Cooper, O. R., Schultz, M. G., Xu, X., Wang, T., Gao, M., Zhao, Y., and
547 Zhang, Y.: Severe surface ozone pollution in China: a global perspective, *Environmental Science &
548 Technology Letters*, 5, 487-494, 2018.
- 549 Lyu, X., Li, K., Guo, H., Morawska, L., Zhou, B., Zeren, Y., Jiang, F., Chen, C., Goldstein, A. H., and Xu,
550 X.: A synergistic ozone-climate control to address emerging ozone pollution challenges, *One Earth*,
551 6, 964-977, 2023.
- 552 Ma, M., Gao, Y., Wang, Y., Zhang, S., Leung, L. R., Liu, C., Wang, S., Zhao, B., Chang, X., and Su, H.:
553 Substantial ozone enhancement over the North China Plain from increased biogenic emissions
554 due to heat waves and land cover in summer 2017, *Atmospheric Chemistry and Physics*, 19, 12195-
555 12207, 2019.
- 556 Seco, R., Holst, T., Davie-Martin, C. L., Simin, T., Guenther, A., Pirk, N., Rinne, J., and Rinnan, R.:
557 Strong isoprene emission response to temperature in tundra vegetation, *Proceedings of the
558 National Academy of Sciences*, 119, e2118014119, 2022.
- 559 Simon, H., Baker, K. R., Akhtar, F., Napelenok, S. L., Possiel, N., Wells, B., and Timin, B.: A direct
560 sensitivity approach to predict hourly ozone resulting from compliance with the National Ambient
561 Air Quality Standard, *Environmental science & technology*, 47, 2304-2313, 2013.
- 562 Wang, H., Lu, X., Seco, R., Stavrakou, T., Karl, T., Jiang, X., Gu, L., and Guenther, A. B.: Modeling
563 isoprene emission response to drought and heatwaves within MEGAN using evapotranspiration
564 data and by coupling with the community land model, *Journal of Advances in Modeling Earth
565 Systems*, 14, e2022MS003174, 2022a.
- 566 Wang, H., Wu, Q., Guenther, A. B., Yang, X., Wang, L., Xiao, T., Li, J., Feng, J., Xu, Q., and Cheng, H.:
567 A long-term estimation of biogenic volatile organic compound (BVOC) emission in China from
568 2001–2016: the roles of land cover change and climate variability, *Atmospheric Chemistry and
569 Physics*, 21, 4825-4848, 2021a.
- 570 Wang, N., Huang, X., Xu, J., Wang, T., Tan, Z.-m., and Ding, A.: Typhoon-boosted biogenic emission
571 aggravates cross-regional ozone pollution in China, *Science Advances*, 8, eabl6166, 2022b.
- 572 Wang, N., Lyu, X., Deng, X., Huang, X., Jiang, F., and Ding, A.: Aggravating O₃ pollution due to
573 NO_x emission control in eastern China, *Science of the Total Environment*, 677, 732-744, 2019.
- 574 Wang, N., Wang, H., Huang, X., Chen, X., Zou, Y., Deng, T., Li, T., Lyu, X., and Yang, F.: Extreme
575 weather exacerbates ozone pollution in the Pearl River Delta, China: role of natural processes,



576 Atmospheric Chemistry and Physics, 24, 1559-1570, 2024a.
577 Wang, N., Du, Y., Chen, D., Meng, H., Chen, X., Zhou, L., Shi, G., Zhan, Y., Feng, M., and Li, W.:
578 Spatial disparities of ozone pollution in the Sichuan Basin spurred by extreme, hot weather,
579 Atmospheric Chemistry and Physics, 24, 3029-3042, 2024b.
580 Wang, N., Xu, J., Pei, C., Tang, R., Zhou, D., Chen, Y., Li, M., Deng, X., Deng, T., Huang, X., and Ding,
581 A.: Air Quality During COVID-19 Lockdown in the Yangtze River Delta and the Pearl River Delta:
582 Two Different Responsive Mechanisms to Emission Reductions in China, Environmental Science &
583 Technology, 55, 5721-5730, [10.1021/acs.est.0c08383](https://doi.org/10.1021/acs.est.0c08383), 2021b.
584 Wang, P., Zhang, Y., Gong, H., Zhang, H., Guenther, A., Zeng, J., Wang, T., and Wang, X.: Updating
585 biogenic volatile organic compound (BVOC) emissions with locally measured emission factors in
586 south China and the effect on modeled ozone and secondary organic aerosol production, Journal
587 of Geophysical Research: Atmospheres, 128, e2023JD039928, 2023.
588 Wang, T., Xue, L., Brimblecombe, P., Lam, Y. F., Li, L., and Zhang, L.: Ozone pollution in China: A
589 review of concentrations, meteorological influences, chemical precursors, and effects, Science of
590 the Total Environment, 575, 1582-1596, 2017.
591 West, J. J., Fiore, A. M., Horowitz, L. W., and Mauzerall, D. L.: Global health benefits of mitigating
592 ozone pollution with methane emission controls, Proceedings of the National Academy of
593 Sciences, 103, 3988-3993, 2006.
594 Wu, K., Yang, X., Chen, D., Gu, S., Lu, Y., Jiang, Q., Wang, K., Ou, Y., Qian, Y., Shao, P., and Lu, S.:
595 Estimation of biogenic VOC emissions and their corresponding impact on ozone and secondary
596 organic aerosol formation in China, Atmospheric Research, 231, 104656,
597 <https://doi.org/10.1016/j.atmosres.2019.104656>, 2020.
598 Xiao, Q., Geng, G., Xue, T., Liu, S., Cai, C., He, K., and Zhang, Q.: Tracking PM_{2.5} and O₃ pollution
599 and the related health burden in China 2013–2020, Environmental science & technology, 56, 6922–
600 6932, 2021.
601 Yin, C., Solmon, F., Deng, X., Zou, Y., Deng, T., Wang, N., Li, F., Mai, B., and Liu, L.: Geographical
602 distribution of ozone seasonality over China, Science of The Total Environment, 689, 625-633,
603 2019.
604 Zhang, X., Huang, T., Zhang, L., Shen, Y., Zhao, Y., Gao, H., Mao, X., Jia, C., and Ma, J.: Three-North
605 Shelter Forest Program contribution to long-term increasing trends of biogenic isoprene
606 emissions in northern China, Atmos. Chem. Phys., 16, 6949-6960, [10.5194/acp-16-6949-2016](https://doi.org/10.5194/acp-16-6949-2016),
607 2016.
608